JOURNAL OF MATERIALS SCIENCE **36** (2001) 399–404

The electro-discharge machining characteristics of TiNi shape memory alloys

H. C. LIN*, K. M. LIN, I. S. CHENG
Department of Materials Science, Feng Chia University, Taichung 407, Taiwan, Republic of China
E-mail: hclin@fcu.edu.tw

The electro-discharge machining (EDM) characteristics of TiNi shape memory alloys (SMAs) have been investigated in this study. Experimental results show that the material removal rate of TiNi SMAs in the EDM process significantly relates to the electro-discharge energy mode, involving the pulse current I_P and pulse duration τ_P. It also has a reverse relationship to the product of the melting temperature and thermal conductivity of TiNi SMAs. In addition, a longer pulse duration τ_P and a lower pulse current I_P should be selected to have a precise EDM machining of TiNi SMAs. Many electro-discharge craters and re-cast materials are observed on the EDM surface of TiNi SMAs. The re-cast layer consists of the oxides TiO_2, $TiNiO_3$ and the deposition particles of the consumed Cu electrode and dissolved dielectric medium. The thickness of the re-cast layer initially increases, reaches a critical value, and then decreases with increasing pulse duration τ_P. The specimen's hardness near the outer surface can reach 750 Hv for EDM TiNi SMAs. This feature originates from the hardening effect of the re-cast layer. The EDM TiNi SMAs still exhibit a nearly perfect shape recovery at a normal bending strain, but a slightly reduced shape recovery at a higher bending strain due to the depression of the re-cast layer. All the $Ti_{49}Ni_{51}$, $Ti_{50}Ni_{50}$ and $Ti_{50}Ni_{40}Cu_{10}$ SMAs exhibit similar EDM characteristics although they have different crystal structures and mechanical properties at room temperature.

1. Introduction

TiNi alloys are an important class of shape memory alloys. They exhibit not only shape memory effect (SME) [1], but also unusual superelasticity [2, 3] and high damping capacities [4, 5]. These properties along with their superior ductility, fatigue strength and corrosion resistance, have resulted in many applications. The basic characteristics of TiNi SMAs, involving transformational crystallography, shape memory phenomena and the effects of thermo-mechanical treatments, have been intensively investigated [6–20]. However, the roadblocks to their development are caused by difficulties in the manufacturing process. It is well known that TiNi alloys can be tensile-deformed in a ductile manner to about 50% strain prior to fracture [1], but the severe strain hardening, high toughness and viscosity, and the unique superelastic behavior have caused the machining characteristics of TiNi SMAs to be quite complicated. Hence, it is difficult to use the conventional machining processes, namely mechanical cutting, drilling and shaping, to machine the TiNi SMAs [21]. To overcome this difficulty, some special techniques, such as the electro-discharge machining and laser machining, may exhibit an excellent ability in machining the TiNi SMAs. However, to the best of our knowledge, few investigations of these special techniques in machining the TiNi SMAs have been reported [22]. EDM is an established application in material processing of metals and ceramics [23–27]. It is an electro-thermal process in which the material is removed by electro-discharges occurring between the work-piece and tool electrode immersed in a liquid dielectric medium. These electro-discharges melt and vaporize minute amounts of the work-piece, which are then ejected and flushed away by the dielectric. Therefore, EDM is an effective technique in machining the stubborn materials, which are difficult to machine by conventional techniques. To extend the applications of TiNi SMAs, some machining technologies for production of complicated shapes with high accuracy should be urgently developed. Hence, the object of this study is to investigate the EDM characteristics of TiNi SMAs. The microstructure, composition and hardness of EDM surfaces are also discussed.

2. Experimental procedure

The conventional tungsten arc-melting technique was employed to prepare the $Ti_{49}Ni_{51}$, $Ti_{50}Ni_{50}$ and $Ti_{50}Ni_{40}Cu_{10}$ alloys. Titanium (purity, 99.7%), nickel (purity, 99.98%) and copper (purity, 99.98%), totaling about 200 g, were melted and remelted at least six times

* Author to whom all correspondence should be addressed.

TABLE I The operational parameters of EDM in this study

Pulse current (A)	6, 12, 25
Pulse duration (μs)	3, 6, 12, 25, 50, 100
Pause duration (μs)	Same value as pulse duration
Gap voltage (V)	50
Electrode	Cu (+); work-piece (−)
Dielectric	Kerosene

in an argon atmosphere. Pure titanium buttons were also melted and used as getters. The mass loss during melting was negligibly small. The as-melted buttons were homogenized at 1050°C for 72 hours in a 7×10^{-6} torr vacuum furnace and then hot-rolled into plates with 5 mm thickness. Specimens for the electro-discharge machining (size: $150 \times 80 \times 5\ mm^3$) were carefully cut and ground from these plates. These specimens were annealed at 800°C for 2 hours in a vacuum furnace and then quenched in water.

The 50-MP type EDM machine, made by Ching-Hung Co. in Taiwan, was conducted to carry out the EDM experiments. The operational parameters are presented in Table I. The microstructures of EDM surfaces were examined using X-ray diffraction (XRD), scanning electron microscopy (SEM) and secondary electron image (SEI). XRD tests were carried out on a Philips PW 1710 XRD using Cu K_α radiation. The power was 40 kV × 30 mA and the 2θ scanning rate was $3^\circ\ min^{-1}$. The morphologies of EDM surfaces were observed using a Philips 515 SEM with SEI facility. The surface hardness was measured in a microvickers tester with a load of 25 g for 15 seconds. For each specimen, the average hardness value was calculated from at least five test readings. The shape memory effect was examined by a bending test [28]. The shape recovery was measured after a complete reverse martensitic transformation.

3. Results and discussion

3.1. The EDM machinability of TiNi SMAs

To investigate the EDM characteristics of $Ti_{49}Ni_{51}$, $Ti_{50}Ni_{50}$ and $Ti_{50}Ni_{40}Cu_{10}$ SMAs, it is helpful to first understand some important metallurgical properties of these alloys. Table II presents the transformation temperatures, hardness, elongation and crystal structures at room temperature for these TiNi alloys. One can find that $Ti_{49}Ni_{51}$, $Ti_{50}Ni_{50}$ and $Ti_{50}Ni_{40}Cu_{10}$ SMAs exhibit B2 phase, B19′ martensite and the mixture of B2, B19 and B19′ phases, respectively. Besides, these TiNi alloys exhibit a soft and ductile behavior.

As well as the material intrinsic properties, many testing parameters, e.g. the electrode polarity, pulse current

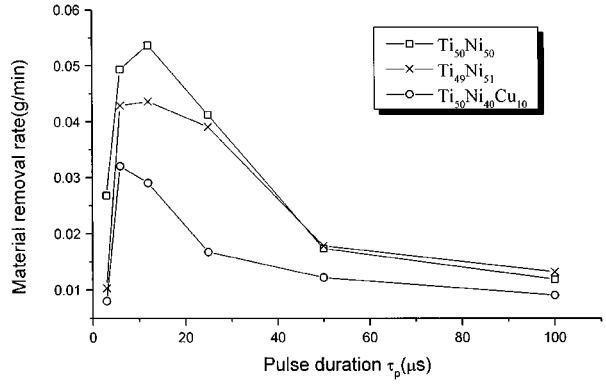

Figure 1 The material removal rate versus the pulse duration τ_P at $I_P = 12$ A for the TiNi SMAs.

I_P, pulse duration τ_P and electrode material, can significantly influence the EDM characteristics. In this study, we hope to understand the effects of pulse current I_P and pulse duration τ_P on the EDM machinability of TiNi SMAs. Fig. 1 shows the material removal rate versus the pulse duration τ_P at $I_P = 12$ A for the TiNi SMAs. It indicates that the material removal rates at various pulse durations τ_P for these alloys exhibit the sequence of $Ti_{50}Ni_{50} > Ti_{49}Ni_{51} > Ti_{50}Ni_{40}Cu_{10}$. This feature is related to their melting temperature and thermal conductivity. Materials with higher melting temperature, leading to less melting and evaporation, and higher thermal conductivity, causing more heat transfer of discharge energy to the nearby matrix, will exhibit a lower material removal rate in EDM. Therefore, the product of the melting temperature and thermal conductivity of materials can be used to predict the machinability of EDM. Table III presents the product of the melting temperature (λ) and thermal conductivity (θ) of the TiNi alloys. The products $\lambda\theta$ for these alloys exhibit the sequence of $Ti_{50}Ni_{50} < Ti_{49}Ni_{51} < Ti_{50}Ni_{40}Cu_{10}$, and hence the material removal rates have the sequence of $Ti_{50}Ni_{50} > Ti_{49}Ni_{51} > Ti_{50}Ni_{40}Cu_{10}$, consistent with the result in Fig. 1. Therefore, one can conclude that the material removal rate has a reverse relationship to the product of λ and θ.

As mentioned above, the electro-discharge energy mode in the EDM process, involving the pulse current

TABLE III The product of the melting temperature and thermal conductivity of TiNi alloys

Alloy	$\lambda\theta$ (W/cm · °C)
$Ti_{50}Ni_{50}$	111.8
$Ti_{49}Ni_{51}$	234.0
$Ti_{50}Ni_{40}Cu_{10}$	314.0

TABLE II The crystal structures and some basic properties of $Ti_{49}Ni_{51}$, $Ti_{50}Ni_{50}$ and $Ti_{50}Ni_{40}Cu_{10}$ SMAs

Alloy	M* (°C)	A* (°C)	Hardness (Hv)	Elongation	Crystal structure
$Ti_{49}Ni_{51}$	−104.35	−60.13	293.2	23%	B2 parent phase
$Ti_{50}Ni_{50}$	34.59	78.84	214.1	25%	B19′ martensite
$Ti_{50}Ni_{40}Cu_{10}$	46.57 (B2 → B19)	69.72 (B19 → B2)	199.7	27%	B2, B19, B19′
	6.23 (B19 → B19′)	22.07 (B19′ → B19)			

M*, A*: DSC peak temperatures of forward and reverse martensitic transformations, respectively.

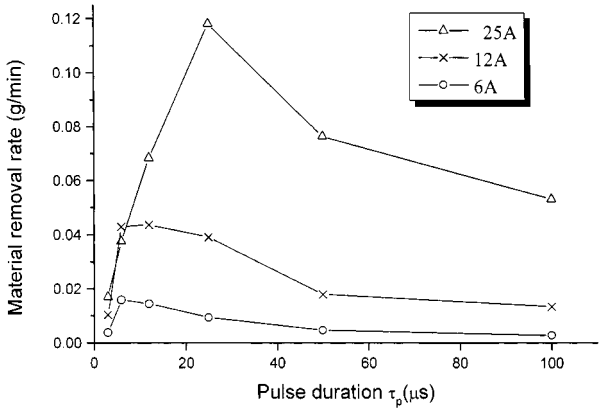

Figure 2 The material removal rate versus the pulse duration τ_P at various pulse currents I_P for the $Ti_{49}Ni_{51}$ alloy.

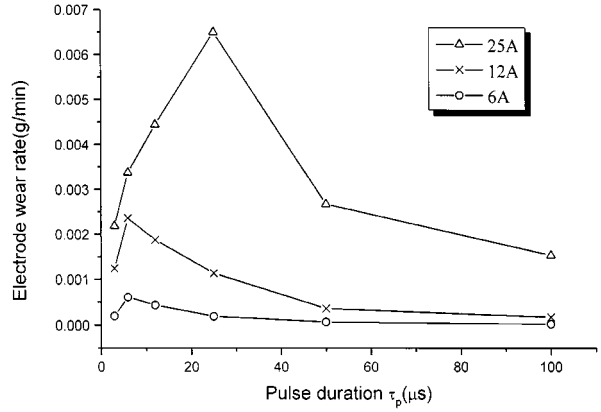

Figure 3 The electrode wear rate versus the pulse duration τ_P at various pulse currents I_P for the $Ti_{49}Ni_{51}$ alloy.

I_P and pulse duration τ_P, will significantly affect the material removal rate. In general, the higher the electro-discharge energy, the higher the material removal rate is expected. Fig. 2 shows the material removal rate versus the pulse duration τ_P at various pulse currents I_P for the $Ti_{49}Ni_{51}$ alloy. It is found that the material removal rate increases with increasing pulse current I_P. It has been reported that the increased pulse current I_P will increase the current density [29]. This feature will obviously increase the material's melting and evaporation and the impact force of expanded dielectric medium. Hence, it is reasonable that the material removal rate increases with increasing pulse current I_P. In addition, one can also find in Figs 1 and 2 that the material removal rates initially increase, reach maximum values, and then decrease with increasing pulse duration τ_P. It is expected that the material removal rate should increase with increasing pulse duration τ_P, because its high accumulated electro-discharge energy will rapidly melt and evaporate the material. However, an over-long pulse duration τ_P will expand the plasma channel [30]. Hence, the EDM covered area is increased and the average energy density is decreased. This feature reduces the material removal rate. Therefore, there appears an optimal pulse duration τ_P, saying $\tau_P = 6$–12 μs in Fig. 1, to have a maximum material removal rate.

As well as the work-piece, the Cu electrode will also slightly melt and evaporate during EDM. To possess the high accuracy and efficiency of EDM, it is important to understand the consumption of electrode material. Fig. 3 shows the electrode wear rate versus the pulse duration τ_P at various pulse currents I_P for the $Ti_{49}Ni_{51}$ alloy. It indicates that the electrode wear rate initially increases, reaches a maximum value and then decreases with increasing pulse duration τ_P. This variation of the electrode wear rate with pulse duration τ_P exhibits a similar tendency to that of the material removal rate with pulse duration τ_P shown in Fig. 2. It indicates that the electro-discharge energy mode will also have a significant effect on the electrode wear rate. Fig. 4 shows the relative electrode wear ratio versus the pulse duration τ_P at various pulse currents I_P for the $Ti_{49}Ni_{51}$ alloy. The relative electrode wear ratio is defined as the ratio of the electrode wear rate to the material removal rate. In Fig. 4, it shows that the relative electrode wear ratio decreases with increasing pulse duration τ_P. It can be explained as below. During EDM, the electro-discharge plasma channel is composed of electron and cation flows. At a short pulse duration τ_P, the electron flow is dominant in the plasma channel and hence the positive electrode, being more attacked by the electrons, has a higher wear rate. However, the ratio of cation flow in the plasma channel increases with increasing pulse duration τ_P [30]. Hence, the material removal rate of the work-piece increases and the relative electrode wear ratio decreases with increasing pulse duration τ_P. As well as the pulse duration τ_P, the pulse current I_P has significant effect on the relative electrode wear ratio. As shown in Fig. 4, a lower pulse current I_P exhibits a lower relative electrode wear ratio. Based on the above discussion, a longer pulse duration τ_P and a lower pulse current I_P should be selected to have a precise EDM machining of TiNi SMAs. In addition, it is worthy to mention that the variations of the material removal rate, electrode wear rate and relative electrode wear ratio with pulse duration τ_P and pulse current I_P for the $Ti_{50}Ni_{50}$ and $Ti_{50}Ni_{40}Cu_{10}$ alloys are similar to those shown in Figs 2–4 for the $Ti_{49}Ni_{51}$ alloy. These features can conclude that the $Ti_{49}Ni_{51}$, $Ti_{50}Ni_{50}$ and $Ti_{50}Ni_{40}Cu_{10}$ SMAs exhibit similar EDM characteristics although they have different crystal structures and mechanical properties at room temperature.

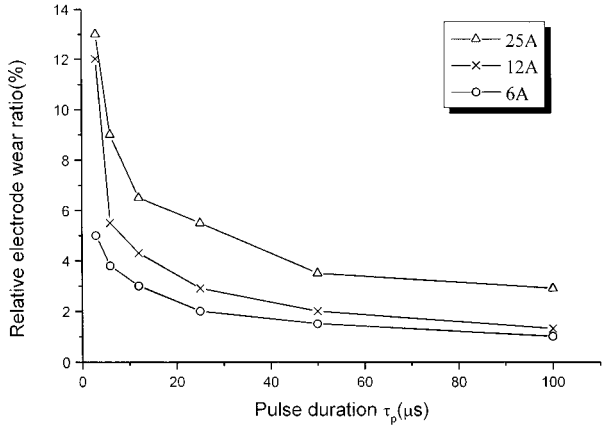

Figure 4 The relative electrode wear ratio versus the pulse duration τ_P at various pulse currents I_P for the $Ti_{49}Ni_{51}$ alloy.

3.2. Microstructures and composition analysis of EDM surfaces of TiNi SMAs

Fig. 5 shows the SEM micrograph of the EDM surface of TiNi SMAs. As indicated in Fig. 5, many electro-discharge craters and re-cast materials are observed on the EDM surface. Fig. 6 shows the XRD patterns of the EDM surface layer for the TiNi SMAs. In indicates that the EDM surface layer consists of TiO_2, $TiNiO_3$, Cu_2O, C and Ni-rich phase. The formation of TiO_2 and $TiNiO_3$ oxides is ascribed to the high activity of Ti and Ni atoms. Cu_2O and C are due to the deposition of the consumed Cu electrode and kerosene dielectric medium. Meanwhile, because Ti atoms are exhausted in forming the TiO_2 particles, the residual Ni atoms diffuse into the TiNi matrix to form the Ni-rich regions. In addition, one can also find in Fig. 5 that lots of cracks occur on the EDM surface. It may be ascribed to the rapid shrinkage of the re-cast materials. Because the re-cast materials exhibit a hard and brittle behavior, it can easily release the shrinkage stress by producing cracks.

As mentioned above, lots of re-cast materials deposit on the EDM surface of TiNi SMAs. Fig. 7a–c show the cross-sectional SEI micrographs near the EDM surface layer for the $Ti_{49}Ni_{51}$ alloy under the conditions of $I_P = 25$ A and $\tau_P = 3, 12, 50$ μs, respectively. The cross-sectional SEI micrographs near the EDM surface layer for the $Ti_{50}Ni_{50}$ and $Ti_{50}Ni_{40}Cu_{10}$ alloys are similar to those shown in Fig. 7a–c and are omitted here. Carefully examining Fig. 7a–c, it indicates that the thickness of the re-cast layer initially increases, reaches a critical value, and then decreases with increasing pulse duration τ_P. This feature comes from the fact that a relatively long pulse duration τ_P will have relatively high electro-discharge energy. This makes more material be melted and re-solidified, as well as more kerosene dielectric medium be dissolved and deposited on the EDM surface. Hence, the thickness of the re-cast layer is increased. However, for an over-long pulse duration τ_P, the extra-high electro-discharge energy will also make the dielectric medium have sufficient impact force to effectively remove the molten materials and the deposited particles away from the EDM surface, and hence the re-cast layer is thinner again.

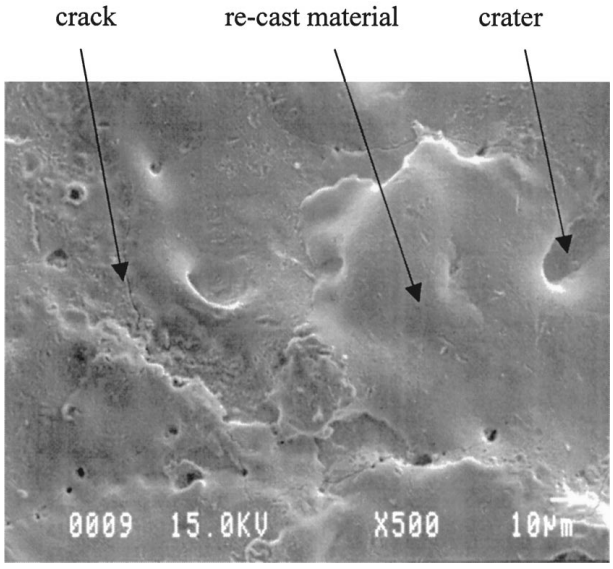

Figure 5 The SEM micrograph of the EDM surface of TiNi SMAs.

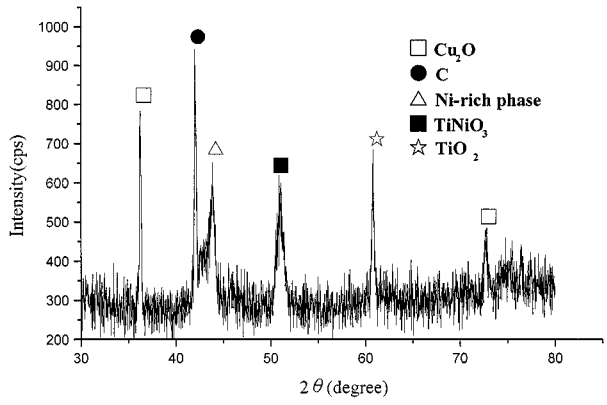

Figure 6 The XRD patterns of the EDM surface layer for the TiNi SMAs.

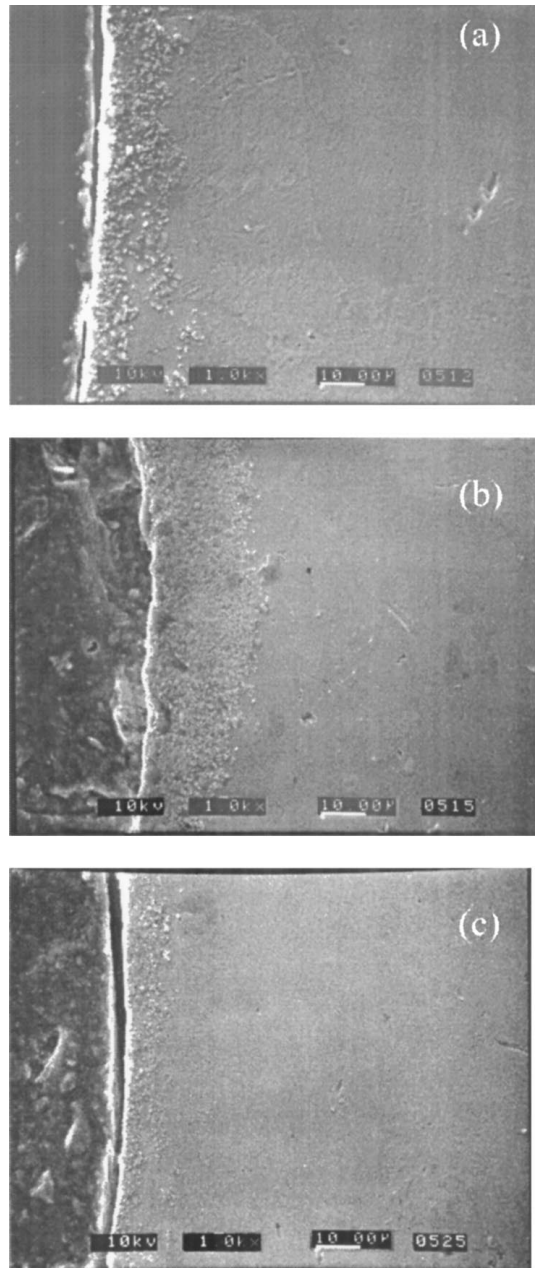

Figure 7 The cross-sectional SEI micrographs near the EDM surface layer for the $Ti_{49}Ni_{51}$ alloy under the conditions of $I_P = 25$ A and $\tau_P =$ (a) 3 μs, (b) 12 μs and (c) 50 μs.

3.3. The hardness and shape recovery ability near EDM surfaces of TiNi SMAs

As discussed in Section 3.2, the re-cast layer formed during the EDM process of TiNi SMAs consists of the oxides TiO_2, TiNiO3 and the deposition particles of the consumed Cu electrode and dissolved dielectric medium. We are interested to understand the hardness and shape recovery ability near the EDM surface of these TiNi SMAs. Fig. 8 shows the specimen's hardness at various distances from the EDM surfaces of $Ti_{49}Ni_{51}$, $Ti_{50}Ni_{50}$ and $Ti_{50}Ni_{40}Cu_{10}$ SMAs under the conditions of $I_P = 25$ A and $\tau_P = 12$ μs. It indicates that the specimen's hardness near the outer surface can reach 750 Hv for these TiNi SMAs. This hardening effect arises from the formation of the oxides TiO_2, $TiNiO_3$ and the deposition particles in the re-cast layer. In addition, the hardness of the TiNi matrix is not affected by the EDM.

Table IV presents the measured shape recovery after a complete reverse martensitic transformation near the EDM surface of TiNi SMAs. The specimen's thickness for SME test is 1.0 mm, which is much thicker than the re-cast layer (<100 μm). It shows in Table IV that the EDM TiNi SMAs exhibit a nearly perfect shape recovery at 3% and 6% bending strains, but a slightly reduced shape recovery at 12% bending strain, as compared with that of as-annealed TiNi SMAs. This feature indicates that the re-cast layer formed during EDM has no obvious effect to depress the shape recovery of TiNi SMAs at normal bending strains. However, at higher bending strains, the shape recovery will be slightly reduced because the re-cast layer does not exhibit the shape memory effect and the constrained effect of the re-cast layer on the TiNi matrix will also depress the shape recovery of the TiNi matrix. Therefore, in the application of thin plates, the re-cast layer on the EDM surface of TiNi SMAs should be mechanically removed before the SME treatment to improve their SME characteristics and to prevent the formation of cracks during the subsequent deformation.

TABLE IV The measured shape recovery, R_{SME}, after a complete reverse martensitic transformation near the EDM surface of $Ti_{49}Ni_{51}$, $Ti_{50}Ni_{50}$ and $Ti_{50}Ni_{40}Cu_{10}$ SMAs

	Shape recovery R_{SME}(%)		
Alloy	$\varepsilon = 3\%$	$\varepsilon = 6\%$	$\varepsilon = 12\%$
$Ti_{50}Ni_{50}$ (as-annealed)	100	100	86
$Ti_{50}Ni_{50}$ (EDM)	100	98	75
$Ti_{49}Ni_{51}$ (as-annealed)	100	100	87
$Ti_{49}Ni_{51}$ (EDM)	100	99	75.5
$Ti_{50}Ni_{40}Cu_{10}$ (as-annealed)	100	100	86.5
$Ti_{50}Ni_{40}Cu_{10}$ (EDM)	100	98	74

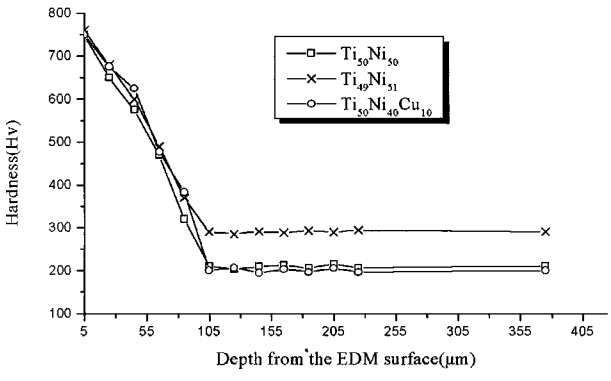

Figure 8 The specimen's hardness at various distances from the EDM surfaces of TiNi SMAs under the conditions of $I_P = 25$ A and $\tau_P = 12$ μs.

4. Conclusions

The EDM characteristics of TiNi shape memory alloys have been investigated in this study. The important conclusions are as follows:

1. The material removal rate of TiNi SMAs in the EDM process significantly relates to the electro-discharge energy mode. It increases monotonically with increasing pulse current, but appears an optimal pulse duration, saying $\tau_P = 6$–12 μs at $I_P = 12$ A in this study, to have a maximum value. Besides, it has a reverse relationship to the product of the melting temperature and thermal conductivity of TiNi SMAs. Meanwhile, a longer pulse duration τ_P and a lower pulse current I_P should be selected to have a precise EDM machining of TiNi SMAs.
2. Many electro-discharge craters and re-cast materials are observed on the EDM surfaces of TiNi SMAs. The re-cast layer consists of the oxides TiO_2, $TiNiO_3$ and the deposition particles of the consumed Cu electrode and dissolved dielectric medium. The thickness of the re-cast layer initially increases, reaches a critical value, and then decreases with increasing pulse duration τ_P.
3. The specimen's hardness near the outer surface can reach 750 Hv for EDM TiNi SMAs. This hardening effect arises from the formation of the oxides TiO_2, $TiNiO_3$ and the deposition particles of the consumed Cu electrode and dissolved dielectric medium in the re-cast layer.
4. The EDM TiNi SMAs still exhibit a nearly perfect shape recovery at a normal bending strain, but a slightly reduced shape recovery at a higher bending strain due to the depression of the re-cast layer.
5. All the $Ti_{49}Ni_{51}$, $Ti_{50}Ni_{50}$ and $Ti_{50}Ni_{40}Cu_{10}$ SMAs exhibit similar EDM characteristics although they have different crystal structures and mechanical properties at room temperature.

Acknowledgement

The authors are pleased to acknowledge the financial support of this research by the National Science Council (NSC), Republic of China, under the Grant NSC88-2216-E-035-007.

References

1. S. MIYAZAKI, K. OTSUKA and Y. SUZUKI, *Scripta Metall.* **15** (1981) 287.
2. S. MIYAZAKI, Y. OHMI, K. OTSUKA and Y. SUZUKI, *J. Phys.* **43** (1982) C4.
3. S. MIYAZAKI, T. IMAI, Y. IGO and K. OTSUKA, *Metall. Trans. A* **17** (1986) 115.
4. H. C. LIN, S. K. WU and M. T. YEH, *ibid.* **24** (1993) 2189.
5. H. C. LIN, S. K. WU and Y. C. CHANG, *ibid.* **26** (1993) 851.

6. T. TADAKI, Y. NAKADA and K. SHIMIZU, *Trans. Jpn. Inst. Met.* **28** (1987) 883.
7. S. MIYAZAKI, Y. IGO and K. OTSUKA, *Acta Metall.* **34** (1986) 2045.
8. S. K. WU, H. C. LIN and T. S. CHOU, *ibid.* **38** (1990) 95.
9. M. NISHIDA and T. HONMA, *Scripta Metall.* **18** (1984) 1293.
10. M. NISHIDA, C. M. WAYMAN and T. HONMA, *ibid.* **18** (1984) 1389.
11. S. K. WU and H. C. LIN, *Scripta Metall. Mater.* **25** (1991) 1295.
12. Y. OKAMOTA, H. HAMANAKA, F. MIURA, H. TAMURA and H. HORIKAWA, *Scripta Metall.* **22** (1988) 517.
13. T. TODOROKI and H. TAMURA, *Trans. Jpn. Inst. Met.* **28** (1987) 83.
14. H. C. LIN, S. K. WU, T. S. CHOU and H. P. KAO, *Acta Metall. Mater.* **39** (1991) 2069.
15. H. C. LIN and S. K. WU, *ibid.* **42** (1994) 1623.
16. E. K. ECKELMEYER, *Scripta Metall.* **10** (1976) 667.
17. R. WASILEWSKI, in "Shape Memory Effects in Alloys," edited by J. Perkin (Plenum, New York, NY, 1975) p. 245.
18. C. M. HWANG, M. MEICHLE, M. B. SALAMON and C. M. WAYMAN, *Philos. Mag.* **47A** (1983) 9.
19. S. K. WU and C. M. WAYMAN, *Metallography* **20** (1987) 359.
20. K. ENAMI, T. YOSHIDA and S. NENNO, *ICOMAT-86* (1987) 103.
21. H. C. LIN, K. M. LIN and Y. C CHEN, *Chinese Journal of Materials Science* **31** (1999) 28.
22. *Idem.*, *Journal of High Temperature Material Processes* **3** (1999) 385.
23. J. S. SONI, *Wear* **177** (1994) 71.
24. L. C. LEE, L. C. LIM, Y. S. WONG and H. H. LU, *J. Materials Processing Technology* **24** (1990) 513.
25. A. G. MAMALIS, G. C. VOSNIAKOS, N. M. VAXEVANIDIS and J. PROHASZKA, *J. Mechanical Working Technology* **15** (1987) 335.
26. Y. FUKUZAWA, Y. KOJIMA, E. SEKIGUCHI and N. MOHORI, *ISIJ International* **33** (1993) 996.
27. M. R. PATEL, M. A. BARRUFET, P. T. EUBANK and D. D. DIBITONTO, *J. Appl. Phys.* **66** (1989) 4104.
28. H. C. LIN and S. K. WU, *Scripta Metall. Mater.* **26** (1992) 59.
29. D. D. DIBITONTO, P. T. EUBANK and M. R. PATEL, *J. Appl. Phys.* **66** (1989) 4095.
30. A. M. GADALLA and B. BOZKURT, *J. Mater. Res.* **7** (1992) 2853.

Received 24 November 1999
and accepted 23 February 2000